IEEE Sensors Council IEEE SENSORS JOURNAL, VOL. 24, NO. 10, 15 MAY 2024

SmartDetect: Safe Driving by Detecting Steering-Wheel Handling With a Single Smartwatch

Rekyan Regasari Mardi Putri, Chin-Chun Chang, *Member, IEEE*, Aditya Fitri Hananta Putra, Setyan Pamungkas, and Deron Liang, *Member, IEEE*

***Abstract*—Holding the steering wheel with both hands is essential for safe driving. This article proposes a novel approach using only one off-the-shelf smartwatch to determine whether the driver is holding the steering wheel with both hands. Two classification models, namely, the individual and universal models, are proposed. An individual model focuses on a particular driver, while the universal model is applicable to all drivers. Both models extract vibration features from the watch's accelerometer signals using the Hilbert–Huang transform and classify the signal pattern by using support vector machines with a radial basis function kernel. Data samples were collected from 35 drivers. The universal model can achieve an accuracy of 98.51% for the hand on which a smartwatch is worn and 90.29% for the hand on which the smartwatch is not worn; the individual model achieves a higher accuracy of 99.21% for the hand on which a smartwatch is worn and 97.18% for the hand on which the smartwatch is not worn.**

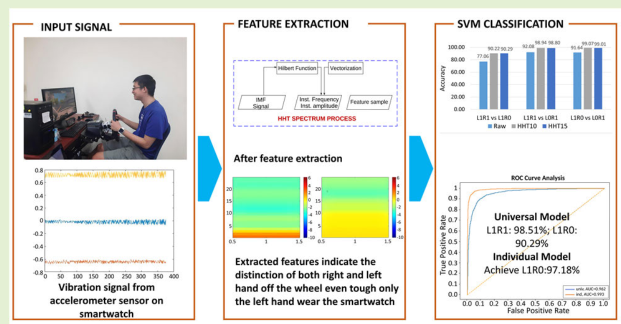

***Index Terms*—Hilbert–Huang transform (HHT), safe driving, steering-wheel handling detection.**

I. Introduction

THE National Highway Traffic Safety Administration (NTHSA) of the United States advises that a driver should operate the steering wheel with both hands while driving to ensure safety. The optimal driving practices to maximize the driver's control of the vehicle and thus reduce the risk of potential accidents involve balancing the steering wheel to avoid sudden movements and minimizing steering wheel reversals [1]. With two hands on the wheel, drivers can exercise far more control in maneuvering the vehicle in the case of a sudden emergency, high speed, or a hard road. However, the driver may not always be aware of the importance of holding the steering wheel for safe driving. Several researches work on safe driving aimed to detect whether the driver's hands are on/off the steering wheel [2], [3].

Several car manufacturing companies (e.g., Tesla, Volkswagen, and BMW) manufacture high-end vehicles with pressure sensors on the steering wheel to address this issue. Such systems can notify the driver if they do not hold the steering wheel with both hands. However, such technology may require years to be applied to lower priced cars. Additionally, the ratio of the number of high-end vehicles to the number of low-end vehicles is 1.56–77.5 million; in other words, high-end vehicles make up only 0.02% of the total number of vehicles [4]. Therefore, an alternative technique to improve the driver's safety applicable for both high-end (new) or low-end (old) cars is required.

Several studies on the recognition of driving behaviors based on different sensing technologies such as cameras [5], [6], [7], [8], [9], pressure distribution sensors [10], and pressure sensors [11] have been developed. According to Statista statistic, published in 2022, smartwatch unit sales worldwide in 2018–2022 have increased drastically until 36%. The emergence of the smartwatch and its popularity in the market can be

Manuscript received 10 January 2024; revised 27 February 2024; accepted 13 March 2024. Date of publication 25 March 2024; date of current version 15 May 2024. The associate editor coordinating the review of this article and approving it for publication was Dr. Hassen Fourati. *(Corresponding author: Rekyan Regasari Mardi Putri.)*

Rekyan Regasari Mardi Putri is with the Department of Computer Science and Information Engineering, National Central University, Taoyuan City 32001, Taiwan, and also with the Department of Informatics Engineering, Brawijaya University, Malang 65145, Indonesia (e-mail: rekyan.rmp@ub.ac.id).

Chin-Chun Chang is with the Department of Computer Science and Engineering, National Taiwan Ocean University, Keelung City 20224, Taiwan (e-mail: cvml@mail.ntou.edu.tw).

Aditya Fitri Hananta Putra is with Astral Web, Taipei City 234-011, Taiwan (e-mail: adityaf.putra@gmail.com).

Setyan Pamungkas was with Pahamify, Bogor 16128, Indonesia. He is now with Nomura Research Institute Indonesia, Jakarta 10220, Indonesia (e-mail: styanpamungkas@gmail.com).

Deron Liang is with the Department of Computer Science and Information Engineering, National Central University, Taoyuan City 32001, Taiwan (e-mail: drliang@csie.ncu.edu.tw).

Digital Object Identifier 10.1109/JSEN.2024.3379486

attributed to its powerful function and ease of use. Forbes 2022 states that the sales of worldwide wearables will double by 2022. The smartwatch contains many different sensors and offers flexibility and extendibility to users, allowing them to install many apps on it. The current applications include healthcare monitoring, day tracking, and notification. Given all these functionalities and the tremendous market growth, it is clear that the use of smartwatches can lead to potential improvement in other domains, such as drivers' safety.

Bi et al. [12] utilized smartwatches and a smartphone in a promising approach called SafeWatch that can warn a driver if any off-steering-wheel action is recognized. Another technology called SafeDrive recognizes various hand movements via an accelerometer and a gyroscope [13]. However, while SafeWatch requires the use of one smartwatch on each hand, SafeDrive requires just one smartwatch with the limitation that the device will have no information regarding the behavior and position of the hand on which a smartwatch is not worn.

This article proposes SmartDetect, a system that uses only one off-the-shelf smartwatch to recognize whether both hands are on the steering wheel. This article found that the vibration patterns of one hand and both hands on the steering wheel as detected by the accelerometer in the smartwatch are different. This is probably because there are two main vibration signal sources, namely, the car engine and hand movement. The signals from each of these sources will weaken or strengthen depending on the position of the hand on the steering wheel. The goal of this article is to capture these signal differences to determine whether both hands are on the steering wheel using one smartwatch. This article proposes two modeling approaches: universal and individual models.

Further, the signals can be classified into three classes: the left and right hands are on the steering wheel (L1R1); the left hand is on the steering wheel, while the right hand is not on the steering wheel (L1R0); and the left hand is not on the steering wheel, while the right hand is on it (L0R1). The Hilbert–Huang transform (HHT) [14] is applied to produce the Hilbert spectrum of the accelerometer signal for feature extraction. Next, support vector machines (SVMs) are employed to build the classification models on the Hilbert spectrum for distinguishing the three classes. The advantage of SVM is that it offers a high classification accuracy since it enables the combination with other pattern classification methods to reach distinct objectives taken in the classification, besides a high accuracy. In other words, it allows the incorporation of tools that transform the biometric signal input data to the SVM and solve the same [15]. In this article, an HHT transformation is applied to the input signal.

Several experiments were conducted to evaluate the proposed methods. The experimental result shows that the individual model can provide 97% average accuracy for L1R1 versus L1R0 and 99.48% average accuracy for L1R1 versus L0R1. Therefore, SmartDetect contributes to a novel approach that can recognize steering-wheel handling detection for both hands using only one smartwatch.

The remainder of this article is organized as follows. Section II provides a background of the research on steering-wheel handling detection. Section III describes the proposed universal and individual models. Section IV presents the experimental results and discussion. Finally, Section V provides the conclusion and prospects of this article.

II. Related Work and Challenges

Technological advances to enhance driver's safety have always been an active research topic [16], [17]. Several works primarily focused on detecting the hand position [2], [3], [12], [13], [18]. The latest approach presented by Bi et al. [12] explored the possibility of relying on the raw signals of a smartwatch. They utilized smartwatches, smartphones, and cameras to capture information on driving behavior. Their system detects whether a hand is holding the steering wheel based on several features from the motion data, such as the posture of the driver's forearm, vibration of the vehicle's body, and vehicle turning. An accuracy of up to 91% was achieved for both precision and recall. The only limitation of their approach is that it can detect the movement of only that hand on which the smartwatch is worn. To recognize the movements of both hands, the driver must wear smartwatches on both hands. SafeWatch applied the vertical component of the vibration signal and did not extract more critical information from the signal. In this study, we applied the HHT to obtain better features.

Furthermore, SafeWatch has more stages than SmartDetect. First, SafeWatch detected the hand movement from the sensor sampling output. Each rest and moving detection result has several distinct processes to detect if the hand is on or off the wheel. Whereas SmartDetect simplifies the process into two main stages: feature extraction and classification. The latest similar research [18] proposed deep learning to predict the driver's hands on/off. However, this article utilizes a less flexible, embedded capacitive sensor than a smartwatch.

The challenges of SmartDetect for steering-wheel handling detection are as follows.

1) It must be convenient, familiar, and feasible, and it should not interfere with driving to improve driver safety; for example, the driver should have to use one smartwatch instead of two.
2) The proposed system should be applicable to various drivers, cars, and environments.
3) It must provide good performance, especially for the hand that is not wearing a smartwatch.

III. System Design

A. System Overview

SmartDetect is a wearable sensing system for improving driver safety. It uses one smartwatch to detect the positions of both hands to determine whether they are on/off the steering wheel. For this purpose, SmartDetect extracts the vibration signal using the three-axes accelerometer of a smartwatch, which is worn on one hand of the driver (the left hand in this article) and which is paired with a smartphone placed in the vehicle. The application scenario is that the smartwatch acts as a sensor for capturing the vibration signals from the car and driver, and then, it sends the captured signals using Bluetooth connection to other devices as a server for analysis. SmartDetect has four parts, as shown in Fig. 1. The first part is

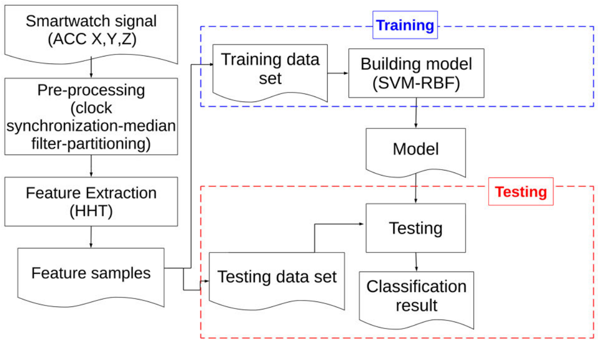

Fig. 1. SmartDetect architecture.

TABLE I
SIGNAL PROCESSING METHOD COMPARISON

Criteria	Fourier	Wavelet	HHT
Basis	A priori	A priori	A posteriori adaptive
Nonlinearity	No	No	Yes
Nonstationary	No	Yes	Yes
Feature extraction	No	Discrete: no; continuous: yes	yes

preprocessing, which involves clock synchronization, median filtering, and signal partitioning. The second part is feature extraction that applies empirical mode decomposition (EMD) and Hilbert spectral analysis (HSA) [14] to extract the HHT features. In the third part, the classification model is learned by SVMs, and testing is conducted in the last part.

B. Signals and Data Samples

The signal was collected from the X-, Y-, and Z-axes accelerometer sensors of the smartwatch in two environments: stationary cars and moving cars. As suggested by Gu et al. [3] and defined by the American Society of Safety Engineers, unsafe driving actions will last for at least 2.5 s. Since the sampling rate of the accelerometer on a smartwatch is 50 Hz, original signals are then obtained for every 125 data points. Therefore, for each action, the sample for each of the three-axis accelerometers comprises 125 data points.

Based on the signal analysis performed, it concluded that driver behavior signals are nonlinear and nonstationary. According to [19], HHT is the most suitable signal transformation method, as shown in Table I. The signals analysis is explained in Figs. 2 and 3. Another research [20] showed that the HHT method is more adaptive than wavelet transform (WT) analysis in analyzing nonstationary magnetotelluric signals and will have a wide application on signal processing.

Fig. 2(a) shows examples of the raw signals of L1R1 and L1R0. According to the mean value of each partitioned sample of the raw signal within a short period, it is evident that the

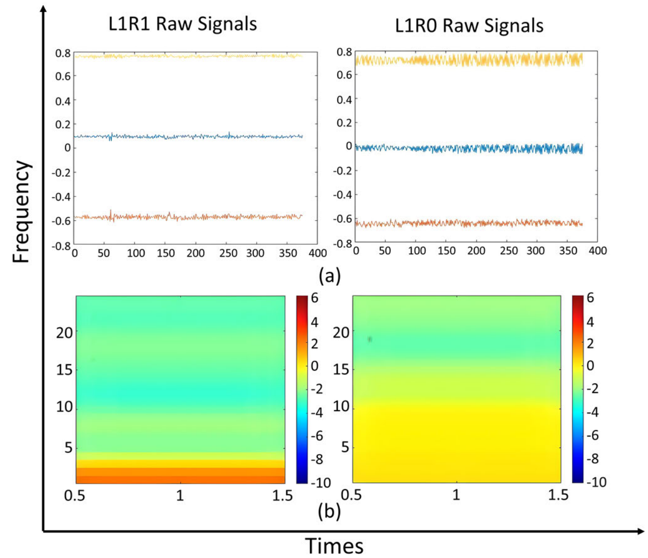

Fig. 2. L1R1 (both hands are on the steering wheel) and L1R0 (the left hand is on the steering wheel, while the right hand is not on the steering wheel): (a) raw signals on three axes and (b) Hilbert spectrum of the x-axis.

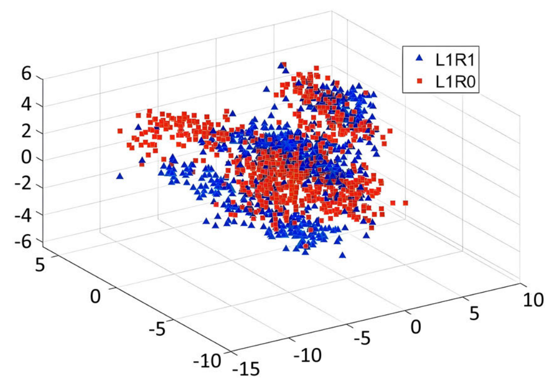

Fig. 3. Feature visualization for sample L1R1 versus L1R0 in 3-D space.

mean value tends to vary with time. This type of signal can be considered a nonstationary signal, and the HHT can be suitable for processing this type of signal. Fig. 2(b) shows the Hilbert spectrum. Fig. 2 demonstrates that although the scenarios with one hand on the wheel and both hands on the wheel have different patterns in both raw signals and Hilbert spectra, it is much harder to distinguish the patterns of the raw signals, whereas the patterns in the Hilbert spectra are drastically different.

Fig. 3 shows the distribution of the three-axis accelerometer signal from the L1R1 (safe action) and L1R0 (unsafe action) classes in the first three components obtained by principal component analysis (PCA). It can be seen that the sample of L1R1 and L1R0 may be not linearly separable, and nonlinear classifiers can be employed.

C. Preprocessing

The preprocessing step is similar to that in [21]. First, the clock of the smartwatch and smartphone is synchronized for partitioning the raw signals. Second, the median filter is applied to the raw signal for noise removal. A median filter

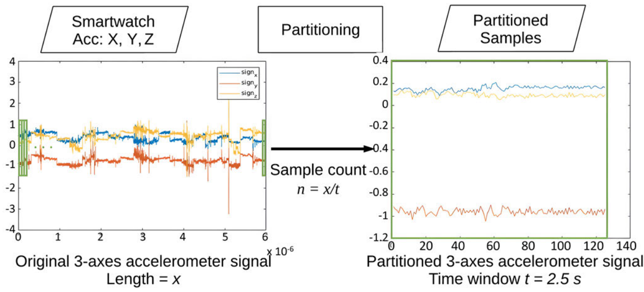

Fig. 4. Data preprocessing result.

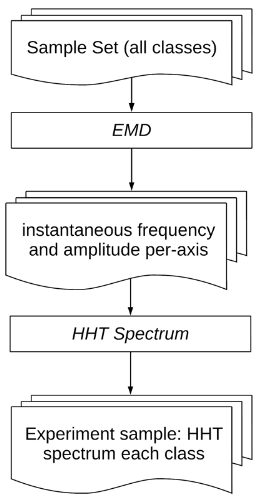

Fig. 5. Feature extraction process.

was applied since it is nonlinear and good to remove noise and extreme values [22], [23].

Third, the raw signal is partitioned into segments as described in Section III-B. Fig. 4 describes the output obtained after partitioning; this output is the preprocessing result.

D. Feature Extraction

Feature extraction aims at extracting effective features for distinguishing safe and unsafe actions. In this stage, the HHT [12], [14], which is often applied to analyze nonstationary and nonlinear data, is used. The feature-extraction process is shown in Fig. 5. It involves two main steps: EMD and HSA that also called HHT spectrum.

EMD decomposes the input signal into several intrinsic mode functions (IMFs) and a residue/trend, which has well-behaved Hilbert transforms. EMD is based on the direct extraction of the energy associated with various intrinsic timescales, the most critical parameters of the system. The essence of the method is to empirically identify the intrinsic oscillatory modes by their characteristic timescales in the data and then decompose the data accordingly. The decomposition is executed with several steps.

1) Identify all the local extrema (maximum and minimum).
2) Connect all the local maximum and minimum by a cubic spline line as the upper and lower envelopes. The time lapse between the maximum and minimum extrema is defined as a characteristic timescale.
3) Obtain the mean value from the envelope of minimum and maximum values, and then decrease the value of signal by the mean value of the envelope.
4) Repeat steps 1–3. If the data were devoid of extrema but contained only inflection points, then it can be differentiated once or more to reveal the extrema, in which the data are decomposed into several IMF components. The final result can be obtained by integration(s) of the components, called IMFs [14].

Then, the Hilbert transform is applied to the IMFs to obtain instantaneous amplitude and frequency data for the IMFs. Such an energy–frequency–time representation of data is designated as the Hilbert spectrum. The Hilbert transform $y(t)$ of a real-valued signal $x(t)$ is defined as [14]

$$y(t) = \frac{1}{\pi} P \int_{-\infty}^{\infty} \frac{x(t')}{t - t'} \mathrm{d}t' \tag{1}$$

where P denotes the Cauchy principal value. It is a method to assign values of certain improper integrals, where a singularity on an integral interval is avoided by limiting the integral interval to the singularity. The Hilbert transform is a companion function for $x(t)$. With $y(t)$, $x(t)$ can be extended to a complex-valued signal $z(t)$ as

$$z(t) = x(t) + iy(t) = a(t)e^{i\theta(t)} \tag{2}$$

where $a(t)$ and $\theta(t)$ are the instantaneous amplitude and phase of $x(t)$, respectively, and they are defined as follows:

$$a(t) = \left(x^2(t) + y^2(t)\right)^{1/2}, \quad \theta(t) = \arctan\left(\frac{y(t)}{x(t)}\right). \tag{3}$$

The instantaneous frequency $f(t)$ can be obtained by

$$f(t) = \frac{\rho \times \omega(t)}{2\pi} \tag{4}$$

where ρ is the sampling rate, and $\omega(t) = ((\partial\theta(t))/\partial t)$ is the instantaneous angular frequency of $x(t)$.

The Hilbert spectrum of three axes (X, Y, and Z) is used as the feature. Each axis has 25 HHT spectra covering 0–25-Hz frequency for each axis. Thus, 75 HHT features can be obtained by averaging the three Hilbert spectra over time.

E. Training and Testing Phases

As mentioned previously, two different modeling approaches, namely, the universal and individual models, were implemented on SVMs. An SVM is a supervised learning algorithm whose objective is to find a hyperplane in the feature space with a large separation margin for classifying the data points.

SVM method classification was utilized according to [24]. This article results suggest that the SVM classifier may perform better than logistic regression (LR), K-nearest neighbor (KNN), and Naïve Bayes (NB). Compared to LR, SVMs can handle nonlinear solutions, whereas LR can only handle linear solutions. Moreover, linear SVMs handle outliers better, as they derives maximum margin solution. Moreover, SVMs take care of outliers better than KNN and outperform KNN when there are large features and lesser training data. It supports after [25] conclusion that SVMs have fast response and

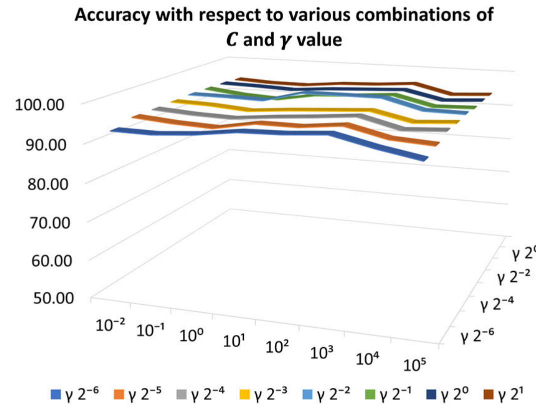

Fig. 6. Accuracy with respect to various combinations of C and γ values.

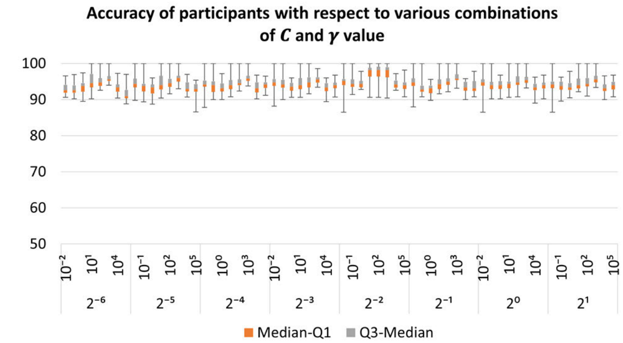

Fig. 7. Accuracy of participants with respect to various combinations of C and γ values.

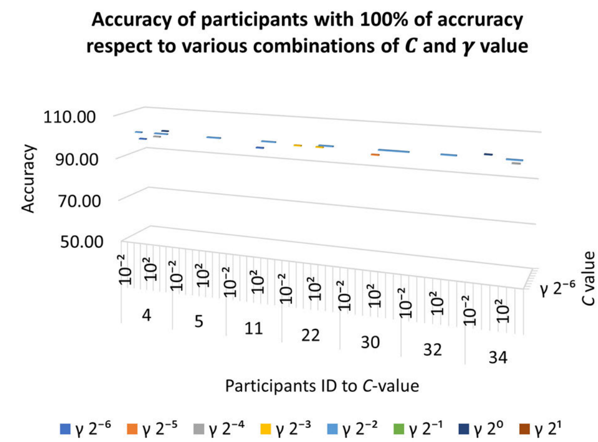

Fig. 8. Participants' accuracy reached 100% with respect to various combinations of C and γ values.

less error, and it is suitable for classifying electromygraphy (EMG) signals compared to NB. The SVM is learned by solving the following optimization problem [26]:

$$\min_{\mathbf{w},b,\varepsilon} \frac{1}{2}\mathbf{w}^{\mathrm{T}}\mathbf{w} + C\sum_{i=1}^{l}\varepsilon_i \tag{5}$$

$$\text{s.t. } y_i(\mathbf{w}^{\mathrm{T}}\phi(\mathbf{x}_i)+b) \geq 0-\varepsilon_i, \quad \varepsilon_i \geq 0 \tag{6}$$

where $C \geq 0$ is the penalty parameter to control the tradeoff between the margin and the error, and $(\mathbf{x}_i, y_i)$ is a training instance-label pair with $\mathbf{x}_i$, which is the ith training vector, and $y_i \in \{-1, 1\}$, which is the associated class label. The sample vector can be nonlinearly mapped by the function ϕ into a higher dimensional feature space.

As explained in Section III-B, the data distributions of safe and unsafe actions are not linearly separable. By the kernel trick, the radial basis function (RBF) kernel [26] can be applied. The RBF kernel $K(\mathbf{x}, \mathbf{y})$ is defined as follows:

$$K(\mathbf{x}, \mathbf{y}) = \exp(-\gamma\|\mathbf{x}-\mathbf{y}\|^2), \quad \gamma > 0 \tag{7}$$

where γ is the hyperparameter for the RBF kernel.

In this article, the best values for the hyperparameters γ and C were selected by fivefold cross-validation; for each cross-validation, 80% of the training sample formed the training set, and the other 20% of the training sample formed the validation set. The parameter sets for C and γ included wide ranges of values, usually covering the appropriate ones for C and γ.

The accuracy of each combination of fivefold cross-validation is described in the graph in Figs. 6–8. Fig. 6 exhibits the stability of the accuracy toward the combinations of C and γ values in a 3-D chart. The boxplot chart in Fig. 7 shows that the accuracy value is stable for each combination of C and γ values, with a minimum accuracy of 86.49 and a maximum of 100%. For the best C and gamma values, the minimum accuracy is 90.40%, and the maximum is 100%. Fig. 8 shows the accuracy stability reaching 100%, where participants achieved 100% accuracy at various values of C and γ, not only at particular values of C and γ.

TABLE II
PARAMETER SET AND THE BEST PARAMETER VALUE

Parameters	Parameter-Value Set	Best Results (Classification's Accuracy)
C	$\{10^{-2}, 10^{-1}, 10^{0}, 10^{1}, 10^{2}, 10^{3}, 10^{4}, 10^{5}\}$	$10^{1}, 10^{2}, 10^{3}$
γ	$\{2^{-6}, 2^{-5}, 2^{-4}, 2^{-2}, 2^{-1}, 2^{0}, 2^{1}\}$	2^{-2}

According to the accuracy result with respect to C and γ values, the γ value 2^{-2} indicates the best classification result up to 100%, and the accuracy is constantly high when the C values are 10^1, 10^2, and 10^3. The best parameter values for C and γ are listed in Table II. Moreover, the results shown in Figs. 6–8 also indicate the robustness of the proposed method.

The universal model was trained on the dataset of all drivers to obtain a single model, whereas the individual model was trained on each driver's data, and each driver had his own model. A preliminary experiment shows that 70% of the collected sample is sufficient for training the model for this application. Accordingly, the training set is 70% of the collected sample selected by stratified random sampling. The other 30% of the collected samples formed the testing set. The average accuracy of the model on the testing data by 25 times of random sampling determined the model's accuracy.

TABLE III
DATA COLLECTION SET

Data collection environment	Participant IDs	number of participants	data set	number of data set	Experiments related	data set used	data length	total data length
Stationary (Old Car)	1 - 35		35		Exp 2, 3, 4, 5	35	1050	
Stationary (New Car)	26 - 35	35	10	48	Exp 6	20	600	1830
Moving (Old Car)	22 - 25		3		Exp 1	6	180	

IV. EVALUATION

A. Experimental Data

The data collection involved 35 participants, where all participants comprised master and Ph.D. students of the Computer Science Department of National Central University (NCU), Taoyuan City, Taiwan; male and female; the ages of the participants were between 22 and 42 years. This range is the medium range of the law ages of driver in Taiwan [32]. For safety, most participants participated in the experiment in a stationary car environment. Three participants, who had a driving license, participated in the experiment in a moving car environment. The stationary car environment was realized in a parked car with the engine running. This environment was used for ascertaining data collection safety, while the moving-car environment was realized in a reserved parking lot on the campus with the university's authorization. The participant profile is summarized in Table III. In the data collection process, each participant was asked to wear a smartwatch on their left wrist and perform three actions: L1R1, L1R0, and L0R1. Each participant conducted each action five times; each action lasted for 2 min. Therefore, each dataset length is 30 min. Table III also summarizes the collected data set that was used as experimental data.

For the moving environment, the participants did not operate the car because of safety concerns. Instead, the participant was seated in the passenger seat and performed hand movements on a fake steering wheel to mimic the driving activities as another individual safely drove the vehicle. In this experiment, we used Mitsubishi Savrin as a representative of old cars (which is a commonly owned old car) and Toyota Corolla Altis 2017 as the new car (a more expensive, newer car) to account for different vibration harshness. For data collection, a commercial standard smartwatch, Sony Smartwatch 3, paired with Sony Xperia Z was used. The sampling rate of the watch is 50 Hz.

The universal and individual models executed three classification scenarios to classify the experiment samples: L1R1 versus L0R1, L0R1 versus L1R0, and L1R1 versus L1R0. The performance evaluation employed accuracy as a metric.

B. Experiments and Results

Six experiments were conducted to prove the claimed contribution. The first experiment was aimed to ensure the feasibility that the experiment was performed on samples collected from the stationary environment instead of the samples from the moving environment. The second experiment aimed to show that the universal model on the HHT features was better than that on the raw signal. The third experiment aimed to analyze the reason why the universal model was ineffective in distinguishing the samples of L1R1 and L1R0 for some participants. The fourth experiment aimed to compare the performances of the universal and individual models. The fifth experiment analyzed the number of features for the individual model. The last experiment was performed to test the individual model on old and new cars, which have different vibration levels.

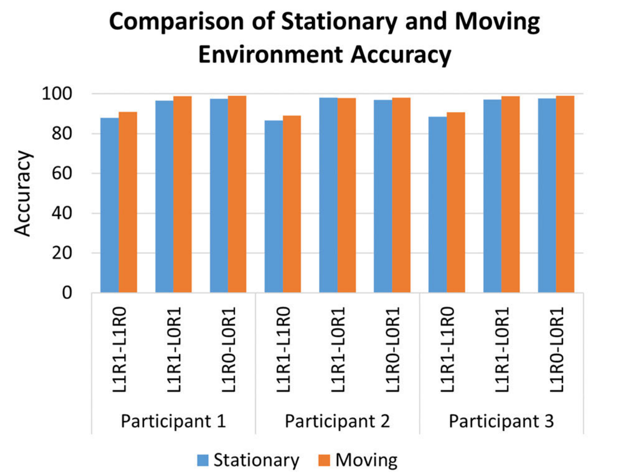

Fig. 9. Comparison of the accuracy of the stationary and moving environments.

To ensure the robustness of the result, random sampling conducted 25 times using different subsets of training and testing sets each time.

1) Comparison of Stationary and Moving Environments: This experiment aimed to ensure that the data from the moving environment could be substituted with the sample from the stationary environment for performance evaluation. This experiment compared the accuracy of the universal model applied to the raw signal from the moving and stationary environments to see if the environment has a significant effect of the accuracy. Data from three participants in the stationary and moving environments were used for this experiment. Fig. 9 shows the comparison result of the accuracies. The complete result of five times random sampling is shown in Table IV.

The null hypothesis of this experiment is that the sample data from the stationary or moving environment present a similar result. A two-tailed t-test with a confidence level of 95% was applied to prove the hypothesis. The result indicates that the t-score value is not in the region of rejection of the null hypothesis, which means the samples of stationary and moving car environments are similar or equal.

TABLE IV
COMPARISON OF THE ACCURACY OF THE STATIONARY AND MOVING ENVIRONMENTS

		STATIONARY	MOVING
L1R1-L1R0	participant 1	87.9	90.86
	participant 2	86.6	89.07
	participant 3	88.53	90.77
L1R1-L0R1	participant 1	96.6	98.78
	participant 2	97.97	97.95
	participant 3	97.05	98.88
L1R0-L0R1	participant 1	97.5	99.08
	participant 2	96.99	98
	participant 3	97.75	98.98

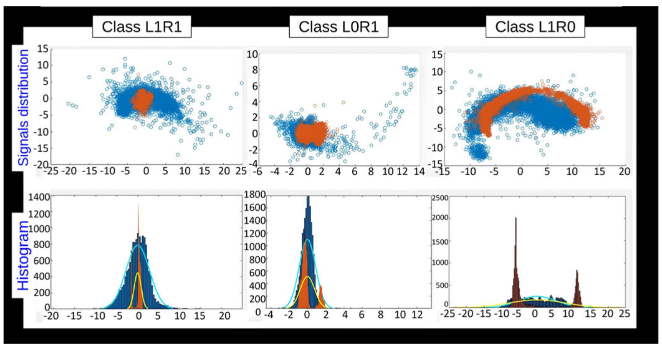

Fig. 10. Analysis of the raw signal pattern, where orange denotes the moving environment, and blue denotes the stationary environment.

More evidences exhibit in Fig. 10. Fig. 10 shows the comparison of the distributions of the raw signals of both environments for each class: L1R1, L0R1, and L1R0. The blue dot denotes the stationary environment, while orange denotes the moving environment. The dimension of the raw signal was reduced by PCA. Fig. 10 indicates that the raw signals on the stationary and moving environments exhibit similar distributions. Fig. 10 also shows that the distribution of the signal on the moving environment is more stable, while that on the stationary environment is more spreading and difficult. The results indicate that if the approach is effective for stationary sample data, then it is suitable for moving car data; for the rest of the experiments, data collected from the stationary car experiment can be used.

However, several previous works resume that speed could affect the vibration of the vehicle or other moving machines. On a hand tractor, velocity strongly affects transmitted vibration to the driver's hands [27]. A study of the rail conveyor's vibration and noise deduces that the conveyor's running speed impacts the vibration and noise [28]. While Zuska and Więckowski [29] discovered that the vibrations of the steering wheel affected when the speed reached 100 km/h. The findings of the references denote that the effect of the car's speed on hand detection on the steering wheel based on the vibration signal of the smartwatch needs to be explored in future work since this experiment utilizes limited data (three participants).

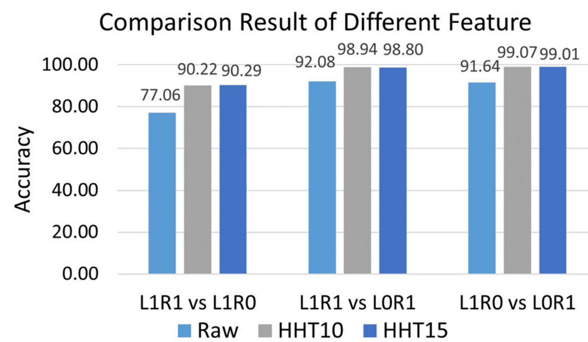

Fig. 11. Comparison of the average accuracies of three different features.

2) Performance Evaluation of Different Features Using the Universal Model: In this experiment, data of 35 participants from the stationary environment using the old car were used. This experiment aimed to prove that HHT feature extraction results perform better than the raw signals. The HHT experiment design was as follows.

1) The compared features were the raw signal, ten HHT features, and 25 HHT features.
2) The universal model and SVMs-RBF classifier were employed. The reasons for using the RBF kernel instead of the linear kernel are explained in Section III-E.
3) Random sampling for training and testing data was performed 25 times to ensure robustness.

These three features were compared. The comparison is shown in Fig. 11. In Fig. 11, the universal model using the HHT extraction feature exhibited a drastic improvement in accuracy. This finding implies that HHT with 25 features gives the best result for all features. Nevertheless, while excellent accuracy is achieved for L1R1–L0R1 and L0R1–L1R0, this is not the case for L1R1–L1R0, representing the hand without a smartwatch (i.e., the right hand in this case). Hence, L1R1–L1R0 accuracy should be improved.

3) Data Distribution Analysis of the User: Since experiment 2 did not yield good results for the hand without a smartwatch (L1R0), the study should analyze the data distribution of the user. The purpose of this experiment was to compare the characteristics of experimental samples to check whether L1R1 and L1R0 have different patterns. PCA was performed for data distribution analysis. The experimental result provides insight into why the classification result from L1R1 against L1R0 cannot be improved, as shown in Fig. 12.

The data used in this analysis comprised the data of 35 participants of the stationary environment experiment using the old car. First, the sample data were split for each driver. Then, PCA reduction was performed for all the drivers, and the mean of the PCA reduction result was calculated. Finally, two results were obtained for each driver—one was the mean value of L1R1, and the other was the mean value of L1R0.

Fig. 12 shows that some data points of L1R1 overlap with the L1R0 data from the other drivers; the other drivers have reverse data between L1R1 and L1R0. Hence, the classifier faces difficulties in distinguishing L1R1 and L1R0 for some

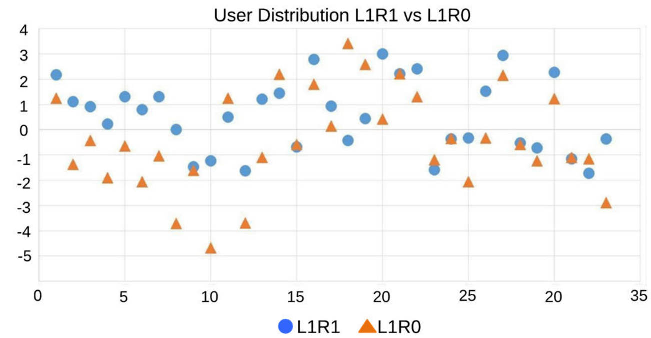

Fig. 12. Distribution analysis of L1R1 and L1R0 for each participant.

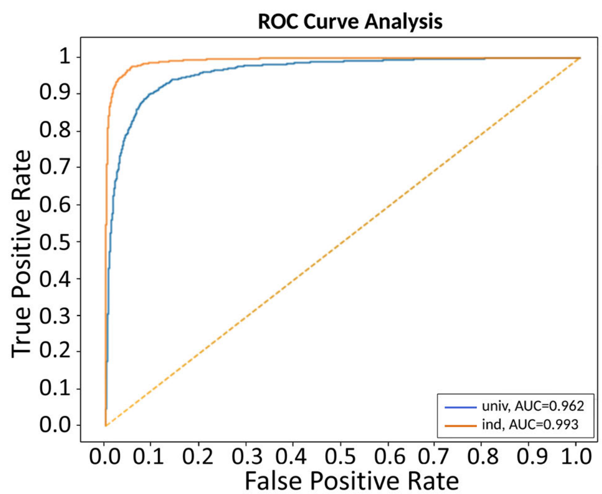

Fig. 13. ROCs for the individual and universal models.

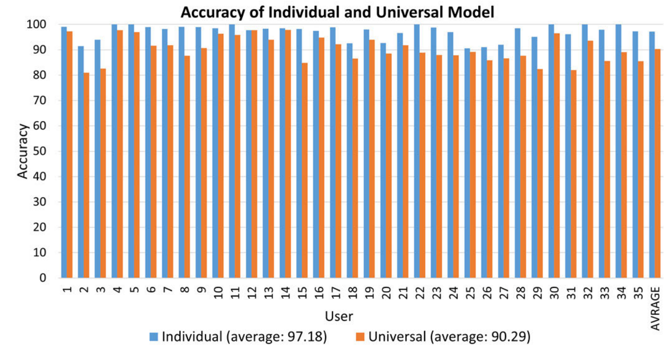

Fig. 14. Accuracy comparison of the individual and universal models of the hand-not-worn smartwatch.

TABLE V
CONFUSION MATRIX

Prediction	Actual (Individual)		Actual (Universal)	
	Positive	Negative	Positive	Negative
Positive	96.77%	2.43%	89.83%	9.25%
Negative	3.23%	97.57%	10.17%	90.75%

data points. The results indicate that L1R1 and L1R0 mean data for every driver are at different levels. Because of the existence of overlap and reverse data between L1R1 and L1R0 of different drivers, the individual model is a proper way to distinguish L1R1 and L1R0.

4) Performance Evaluation of the Individual Model: This experiment aims to evaluate the performance of the proposed individual models and whether they can provide better accuracy on L1R1–L1R0 than the universal model. This experiment was designed with the individual model as explained in Section III. System design uses 25 HHT features and the SVMs-RBF classifier, and the experiment was run 25 times with random sampling. The data used in this experiment comprised the data of 35 participants in the stationary environment experiment using the old car. The performance was analyzed using the receiver operating characteristic (ROC) curve, as shown in Fig. 13. It was applied because the observations were balanced between each class, both L1R1 and L1R0. The ROC curve summarizes the tradeoff between the true-positive and false-positive rates for a predictive model using different probability thresholds. It is ideal if the area under the curve (AUC) approaches 1 (meaning the curve is far away from the cross line, or the yellow dotted line), and it performs poorly if the AUC is close to 0.5 (meaning the curve approaches the cross line).

Fig. 13 shows that the individual model provides better results than the universal model on the hand which not worn smartwatch. An ROC curve closer to (0,1) is desirable because how good a model is at predicting the positive class when the actual outcome is positive that is remarkably higher than how often a positive class is predicted when the actual outcome is negative. The AUC of the individual model is 0.993, which is better than the AUC of the universal model (0.962). This result indicates that a classifier's probability of ranking a randomly chosen positive instance is higher for the individual model than for the universal.

Fig. 14 shows the accuracy for each user, and it shows that there is no significant difference among the participants. The average accuracy of the individual model is 97.18%, with a standard deviation of 2.89, while the average accuracy of the universal model is 90.29% with a standard deviation of 5.05. A confusion matrix consisting the rate of true positive, false positive, false negative, and true negative is provided in Table V, where the positive is L1R1, and the negative is L1R0. The performance measures indicate that the individual model is more accurate than the universal model.

The comparison of individual and universal models' accuracy for the hand-worn smartwatch is observed by L1R1–L0R1 classification. The result is shown in Fig. 15. The result is quite similar because the difference between the hand-worn smartwatch when it is on or off the wheel is significant. Therefore, the result of the universal model is good, and the individual model improves a few results. However, the individual model solved the challenge of distinguishing the position of the hand-not-worn smartwatch, according to the results shown in Figs. 13 and 14.

In the experiments with the individual model, the minimum count of data to be processed was four—two from L1R1

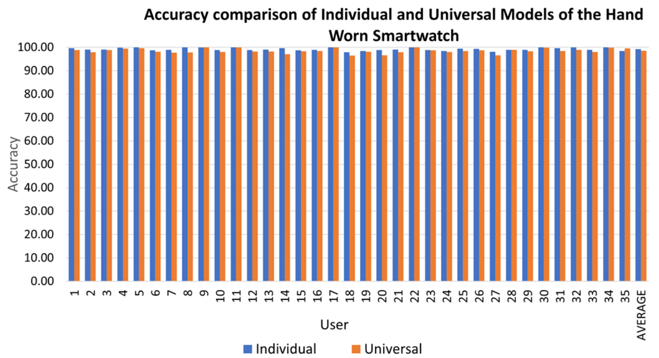

Fig. 15. Accuracy comparison of the individual and universal models of the hand-worn smartwatch.

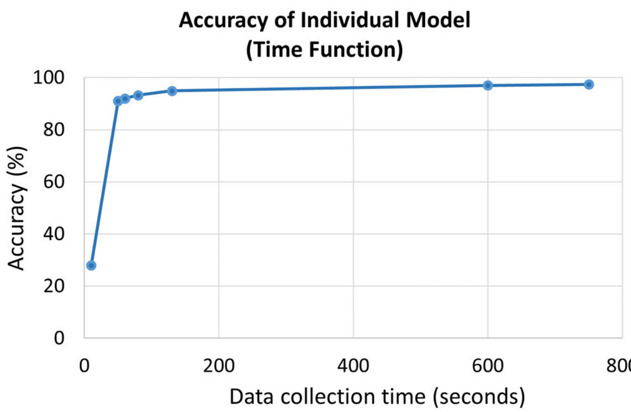

Fig. 16. Accuracy of the individual model with respect to the signal length.

and two from L1R0, and the minimum duration was 10 s. However, the minimum data size and length result in poor model performance. We obtained better performances with longer data lengths. The accuracy was greater than 90% for data samples of length 50 s (20 data), 92% for 60 s, 93.3% for 80 s, 94.92% for 130 s, and approximately 97% for 600 s. Fig. 16 shows the accuracy plotted as a function of time; the confidence interval is 97.18 $\pm$ 1.89, with a confidence level of 95% for 600–750 s of data collection time.

When applied the HHT on partitioned signals, a spectral leakage possibly occurs, though the good result of this experiment shows that spectral leakage is not severe for this application. However, overcoming the spectral leakage will be one of the future works. For example, a modified HHT [30] can be adopted.

5) Dominant Feature Analysis: In this experiment, the dominant feature and the number of features were analyzed for the individual model. The results provide an insight into the effect of the number of features on system accuracy. The dominant features were analyzed by two strategies: 1) feature ranking—the feature importance was determined from the absolute value of the feature weight given by the linear SVM [31] and 2) PCA.

The experimental results are summarized in Table VI. As seen from Table VI, the system accuracy can be maintained by retaining approximately two-third of the important features or principal components.

TABLE VI
ANALYSIS OF DOMINANT FEATURES

Feature	Accuracy (individual model)			
	Min	Max	Average	SD
All 75 features	90.58	100.00	97.18	2.89
55 important features by feature ranking	92.57	100.00	97.36	2.32
The first 50 principal components	90.05	99.90	97.09	2.86

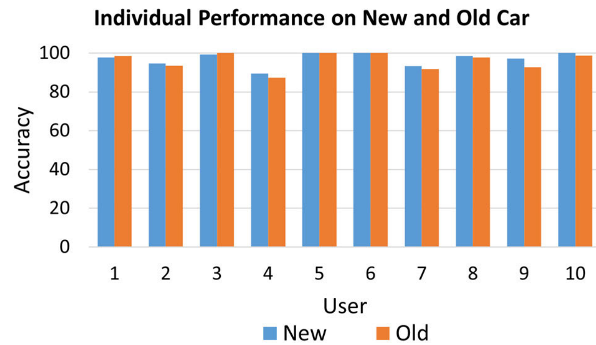

Fig. 17. Individual model performances for new and old cars.

6) Comparison of Old-Car and New-Car Environments: This experiment was designed to check whether the individual model is effective for both old and new cars to allay the suspicion that different vibrations from different vehicles will affect the accuracy. This experiment was conducted by using an individual model with ten participants who drove both old and new cars in a stationary environment. In all, 75 HHT features were used, and the classifier was SVMs-RBF. The process is the same as that for the individual model for each driver on an old or new car. For the ten participants, the old-car models and new-car models were labeled MO_1–MO_{10} and MN_1–MN_{10}, respectively.

The experimental models achieved an accuracy average of 97.05 with a standard deviation of 3.49 for the new car and an average of 96.03 with a standard deviation of 4.38 for the old car. The result is shown in Fig. 17. This result provides convincing evidence that the pattern is similar for most participants; the model performance of only participant number 9 was slightly different. This result is reasonable because even for the same type of car, the accuracy may differ slightly with the participants because the dataset was obtained randomly from the behavior. In addition, the vibration signal patterns were similar even for different amplitudes. This experiment proved that the suspicion that vibration will affect the performance is unwarranted and that the individual model is robust and applicable to diverse situations as it can handle vibrations of different amplitudes.

V. CONCLUSION

Universal and individual models with HHT feature extraction and SVMs-RBF are presented as a novel approach that employs only one smartwatch to detect steering-wheel handling for both hands. The main challenge is to detect the behavior of the hand on which the smartwatch is not worn. The individual model can solve this problem well, and it achieves an AUC of 0.993 for the ROC curve and an average accuracy of 97.36%. This approach requires new data collection to train a new model for each new user and around 60–600 s of data for achieving an accuracy between 91% and 97.18%. The universal model is more feasible for practical use because it does not need to learn the signal patterns of each new user, but it provides a limited accuracy of 90.29% with an AUC of 0.962.

The experiments and result analysis prove that although stationary data were used to avoid dangerous situations involving data collection in a moving-car environment, the proposed approach is effective for moving-car environments. Nevertheless, the data for this experiment is limited. A deep study of vibration signal in stationary and some speed degrees of moving car will be valuable.

The proposed approach is generalizable for many drivers as the research involved 35 participants and provided strong model performance. The participants' age range did not cover the ages 18–21 and 43–65, as stated in the law ages of driver in Taiwan [32]. It will be more meaningful to cover the ages of the possible driver in the future work.

Further, the approach is suitable for high-end cars (i.e., new cars) as well as average-level cars (old cars). In future works, ways to overcome spectral leakage and a deep analysis of the essential features will be valuable.

References

[1] U.S. Department of Transportation (USDOT), National Highway Traffic Safety Administration (NHTSA). *Using Efficient Steering Technique*. Accessed: Apr. 20, 2020. [Online]. Available: https://www.nhtsa.gov/sites/nhtsa.dot.gov/files/steeringtechniques.pdf

[2] H. Chen, Z. Yang, C. Huang, and Q. Zhang, "Drive safe inspector: A wearable-based fine-grained technique for driver hand position detection," in *Proc. IEEE Global Commun. Conf. (GLOBECOM)*, Abu Dhabi, United Arab Emirates, Dec. 2018, pp. 1–7, doi: 10.1109/GLOCOM.2018.8647653.

[3] Y. Gu, Y. Song, I. Goncharenko, and S. Kamijo, "Driver hand activity recognition using NIR camera and deep neural network," in *Proc. IEEE 4th Global Conf. Life Sci. Technol. (LifeTech)*, Osaka, Japan, Mar. 2022, pp. 299–300, doi: 10.1109/LifeTech53646.2022.9754956.

[4] U.S. Department of Transportation, Bureau of Transportation Statistics. (2017). *Transportation Statistic Annual Report 2017*. Washington, DC, USA. [Online]. Available: https://www.bts.gov/bts-publications/transportation-statistics-annual-reports/tsar-2017

[5] J. W. Baek, B.-G. Han, K.-J. Kim, Y.-S. Chung, and S.-I. Lee, "Real-time drowsiness detection algorithm for driver state monitoring systems," in *Proc. 10th Int. Conf. Ubiquitous Future Netw. (ICUFN)*, Jul. 2018, pp. 73–75, doi: 10.1109/ICUFN.2018.8436988.

[6] Y. Katyal, S. Alur, and S. Dwivedi, "Safe driving by detecting lane discipline and driver drowsiness," in *Proc. IEEE Int. Conf. Adv. Commun., Control Comput. Technol.*, May 2014, pp. 1008–1012, doi: 10.1109/ICACCCT.2014.7019248.

[7] O. Wathiq and B. D. Ambudkar, "Optimized driver safety through driver fatigue detection methods," in *Proc. Int. Conf. Trends Electron. Informat. (ICEI)*, May 2017, pp. 68–73, doi: 10.1109/ICOEI.2017.8300787.

[8] H. A. Abosaq et al., "Unusual driver behavior detection in videos using deep learning models," *Sensors*, vol. 23, no. 1, p. 311, Dec. 2022, doi: 10.3390/s23010311.

[9] E. Mantouka, E. Barmpounakis, E. Vlahogianni, and J. Golias, "Smartphone sensing for understanding driving behavior: Current practice and challenges," *Int. J. Transp. Sci. Technol.*, vol. 10, no. 3, pp. 266–282, 2021.

[10] M. Ding, T. Suzuki, and T. Ogasawara, "Estimation of driver's posture using pressure distribution sensors in driving simulator and on-road experiment," in *Proc. IEEE Int. Conf. Cyborg Bionic Syst. (CBS)*, Oct. 2017, pp. 215–220, doi: 10.1109/CBS.2017.8266102.

[11] H. A. Rahim, Z. M. Yusop, S. D. Bin Syed Hassan, and C. K. Seng, "Grasp hand approach to detect the attentiveness and fatigue of driver via vibration system," in *Proc. 6th Int. Colloq. Signal Process. Appl.*, May 2010, pp. 1–5, doi: 10.1109/CSPA.2010.5545240.

[12] C. Bi, J. Huang, G. Xing, L. Jiang, X. Liu, and M. Chen, "SafeWatch: A wearable hand motion tracking system for improving driving safety," *ACM Trans. Cyber-Phys. Syst.*, vol. 4, no. 1, pp. 1–21, 2020, doi: 10.1145/3360323.

[13] L. Jiang, X. Lin, X. Liu, C. Bi, and G. Xing, "SafeDrive: Detecting distracted driving behaviors using Wrist-Worn devices," *Proc. ACM Interact., Mobile, Wearable Ubiquitous Technol.*, vol. 1, no. 4, pp. 1–22, 2018, doi: 10.1145/3161179.

[14] N. E. Huang et al., "The empirical mode decomposition and the Hilbert spectrum for nonlinear and non-stationary time series analysis," *Proc. Roy. Soc. London A, Math., Phys. Eng. Sci.*, vol. 454, no. 1971, pp. 903–995, Mar. 1998.

[15] D. C. Toledo-Pérez, J. Rodríguez-Reséndiz, R. A. Gómez-Loenzo, and J. C. Jauregui-Correa, "Support vector machine-based EMG signal classification techniques: A review," *Appl. Sci.*, vol. 9, no. 20, p. 4402, Oct. 2019, doi: 10.3390/app9204402.

[16] L. Liu et al., "Toward detection of unsafe driving with wearables," in *Proc. Workshop Wearable Syst. Appl.*, 2015, pp. 27–32.

[17] B.-G. Lee, B.-L. Lee, and W.-Y. Chung, "Wristband-type driver vigilance monitoring system using smartwatch," *IEEE Sensors J.*, vol. 15, no. 10, pp. 5624–5633, Oct. 2015.

[18] H. Pyeon, H. Kim, R. C. Kim, G. Oh, and S. Lim, "Deep learning-based driver's hands on/off prediction system using in-vehicle data," *Sensors*, vol. 23, no. 3, p. 1442, 2023, doi: 10.3390/s23031442.

[19] N. E. Huang and Z. Wu, "A review on Hilbert–Huang transform: Method and its applications to geophysical studies," *Rev. Geophys.*, vol. 46, no. 2, pp. 1–2, 2008.

[20] X. Cai and J. Cai, "Comparison of WHT and HHT methods for analyzing magnetotelluric signal," in *Proc. 9th Int. Conf. Fuzzy Syst. Knowl. Discovery*, Chongqing, China, May 2012, pp. 1769–1773, doi: 10.1109/FSKD.2012.6233952.

[21] R. R. Mardi Putri, C.-H. Yang, C.-C. Chang, and D. Liang, "Smartwatch-based open-set driver identification by using GMM-based behavior modeling approach," *IEEE Sensors J.*, vol. 21, no. 4, pp. 4918–4926, Feb. 2021, doi: 10.1109/JSEN.2020.3030810.

[22] M. Kaufmann, "Video signal processing," in *Digital Video and HD*, 2nd ed. Amsterdam, The Netherlands: Elsevier, 2012, pp. 377–388, doi: 10.1016/B978-0-12-391926-7.50031-X.

[23] K. M. Sagayam, P. M. Bruntha, M. Sridevi, M. R. Sam, U. Kose, and O. Deperlioglu, "A cognitive perception on content-based image retrieval using an advanced soft computing paradigm," in *Advanced Machine Vision Paradigms for Medical Image Analysis*. New York, NY, USA: Academic, 2020, ch. 7, pp. 189–211, doi: 10.1016/B978-0-12-819295-5.00007-X.

[24] M. Y. Hossain and A. Sayeed, "A comparative study of motor imagery (MI) detection in electroencephalogram (EEG) signals using different classification algorithms," in *Proc. Int. Conf. Autom., Control Mechatronics Ind. 4.0 (ACMI)*, Rajshahi, Bangladesh, Jul. 2021, pp. 1–6, doi: 10.1109/ACMI53878.2021.9528276.

[25] Y. Narayan, "Comparative analysis of SVM and Naive Bayes classifier for the SEMG signal classification," *Mater. Today: Proc.*, vol. 37, pp. 3241–3245, Jan. 2020, doi: 10.1016/j.matpr.2020.09.093.

[26] C. H. Hsu, C. C. Chang, and C. J. Lin, "A practical guide to support vector classification," Dept. Comput. Sci., Nat. Taiwan Univ., Taiwan, Tech. Rep., 2016, pp. 1–12.

[27] A. Ali, M. Abdullah, A. Hamid, and A. Fahem, "Effect of steering wheel vibration on drivers hands in a two-wheel drivers hand tractor," *J. Eng.*, vol. 17, no. 6, pp. 1539–1549, 2011.

[28] N. Hao, X. Sun, M. Zhang, Y. Zhang, X. Wang, and X. Yi, "Vibration and noise analysis and experimental study of rail conveyor," *Sensors*, vol. 23, no. 10, p. 4867, May 2023, doi: 10.3390/s23104867.

[29] A. Zuska and D. Wieckowski, "The impact of unbalanced wheels and vehicle speed on driving comfort," in *Proc. XI Int. Sci.-Tech. Conf. Automot. Saf.*, Žastá, Slovakia, Apr. 2018, pp. 1–6, doi: 10.1109/AUTOSAFE.2018.8373310.

[30] X. Shan et al., "A revised Hilbert–huang transformation to track non-stationary association of electroencephalography signals," *IEEE Trans. Neural Syst. Rehabil. Eng.*, vol. 29, pp. 841–851, 2021.
[31] H. Xing, M. Ha, B. Hu, and D. Tian, "Linear feature-weighted support vector machine," *Fuzzy Inf. Eng.*, vol. 1, no. 3, pp. 289–305, Sep. 2009.
[32] *How to Apply for a Locally Issued Taiwan Driver's License—Travel Taiwan During Covid-19*. Accessed: Apr. 20, 2020. [Online]. Available: https://www.traveltaiwanduringcovid19.com/1604/how-to-get-taiwan-drivers-license/

Rekyan Regasari Mardi Putri received the B.S. degree in electrical engineering from ITS, Surabaya, Indonesia, in 1995, and the M.S. degree in electrical engineering from Brawijaya University, Malang, Indonesia, in 2010. She is currently pursuing the Ph.D. degree with the Department of Computer Science and Information Engineering, National Central University (NCU), Taoyuan City, Taiwan.

Her research interests include machine learning, decision support system, and driver recognition.

Chin-Chun Chang (Member, IEEE) received the B.S., M.S., and Ph.D. degrees in computer science from National Chiao Tung University (NCTU), Hsinchu, Taiwan, in 1989, 1991, and 2000, respectively.

From 2001 to 2002, he was a Faculty Member with the Department of Computer Science and Engineering, Tatung University, Taipei, Taiwan. In 2002, he joined the Department of Computer Science and Engineering, National Taiwan Ocean University (NTOU), Keelung City, Taiwan, where he is currently an Associate Professor. His research interests include computer vision, machine learning, and pattern recognition.

Aditya Fitri Hananta Putra received the master's degree from National Central University, Taoyuan City, Taiwan, in 2018.

He is currently a Web/Magento Developer with Astral Web, Taipei City, Taiwan. His research interests include intelligent systems.

Setyan Pamungkas received the master's degree from National Central University, Taoyuan City, Taiwan, in 2019.

He was an Engineer with Pahamify, Bogor, Indonesia. His research interests are machine learning.

Deron Liang (Member, IEEE) received the B.S. degree in electrical engineering from NTU, Taipei, Taiwan, in 1983, and the M.S. and Ph.D. degrees in computer science from the University of Maryland, College Park, MD, USA, in 1991 and 1992, respectively.

Since 2008, he has been a Faculty Member with the Department of Computer Science and Information Engineering and also serves as the Director for the Software Research Center, National Central University (NCU), Taoyuan, Taiwan. His current research interests are in the areas of software fault tolerance, system security, and system reliability analysis.

Dr. Liang is a member of ACM.